Electronic Supporting Information

Film-electrochemical EPR spectroscopy to investigate electron transfer in membrane proteins in their native environment

Davide Facchetti[a], Yunfei Dang[a] , Maryam Seif-Eddine[a,b], Blaise L. Geoghegan[a] and Maxie M. Roessler[a]*

[a.] *Department of Chemistry, Imperial College London, Molecular Sciences Research Hub, White City Campus, Wood Lane, London W12 0BZ, UK.*
[b.] *CNRS: Marseille, Bioénergétique et Ingénierie des Protéines (BIP), 31 Chemin Joseph Aiguier, 13009, Marseille, France.*
** E-mail: m.roessler@imperial.ac.uk*

Contents

1 Materials and Methods

The following materials were purchased form Sigma Aldrich: Ti foil (99.7% trace metals basis, thickness 0.25 mm), indium tin oxide (ITO) nanoparticles (<50 nm diameter), methanol, isopropanol, acetone, sodium chloride, potassium chloride, phosphate-buffered saline (PBS) buffer tablets, acetic acid, ethanol, 4-aminoTEMPO, 1-[3 (dimethylamino)propyl]-3-ethylcarbodiimide hydrochloride (EDC), N-hydroxysuccinimide (NHS), 3-phosphonopropionic acid, 3-Aminopropylphosphonic acid, triethylamine (NEt_3). Polybead® Microspheres, 750 nm diameter, 2.54% w/v suspension in water, were purchased from Polysciences Europe GmbH (Germany).

Titanium wire (Ti, 98%, outer diameter (O.D.) 0.320 μm, Advent Research Materials) was used to connect the mesoITO working electrode to the potentiostat. The titanium wire was connected to the electrode by folding the top 0.5 cm of the Ti strip and clipping onto the wire. Stainless steel (AISI 316L) hollow tube (outside diameter: 2.1mm, wall thickness: 0.25mm, inside diameter: 1.6mm) was used as a counter electrode and purchased from Goodfellow Cambridge Limited (Huntingdon, UK). Ag wire served as pseudo-reference electrode (98%, O.D. 0.125 μm, Advent Research Materials).

2 Production and characterisation of IMVs

E. coli cells with an expression vector for MsrQ were obtained from the KEIO collection[1] (*E.coli* K12 AG1 with expression vector pCAN-24) and kindly provided by Dr Cassandra Backes and Prof. Filipe Cabreiro (University of Köln). Cells were grown aerobically at 37 °C in 2L Erlenmeyer flasks and MsrQ overexpression was induced with 0.1 mM Isopropyl β-d-1-thiogalactopyranoside (IPTG) following the protocol reported in the literature.[2] Briefly, cells were grown in 0.4 L of terrific broth in each flask and overexpression was started at an OD of 0.7. The temperature was lowered to 30 °C and the cells were

harvested after 16 hours. Each flask provided on average 3g of wet cells after harvesting. IMVs were isolated with a sequential centrifugation protocol and filtered on a 55% sucrose cushion as described previously.[3] Ultracentrifugation speed and concentration of sucrose and EDTA were selected to reduce the likelihood of particle aggregation[4] and to limit the inversion of the membranes[5,6]. At the concentration used in our study, EDTA has been shown to not interfere with the protein structure and to facilitate the IMVs isolation.[7] Dynamic light scattering (DLS) measurements were performed on a Malvern Panalytical Zetasizer Ultra, using a small volume cuvette (60 µL). Transmission electron microscopy (TEM) images were collected with a Tecnai 12 Spirit. Samples were negatively stained with uranyl acetate. In all the experiments involving IMVs, the particles were dispersed in MOPS 100 mM-EDTA 5 mM pH 7.0. The samples had a total protein concentration of 30 mg/mL as determined with a modified Lowry assay.[8]

3 Preparation of working electrodes and electrochemical set-up

The Ti strips were laser-cut into desired shapes from the Ti foil (length 4.5 cm, width 0.1 or 0.2 cm). All the electrodes used for experiments reported in the main paper had a width of 1 mm. 2 mm electrodes were used during the set-up optimisation and were used for the experiments shown in ESI Figure 3c and ESI Table 1. The Ti strips used for the preparation of working electrodes were sputtered at room-temperature with a HEX-L sputtering system (Korvus Technology, UK) using the following parameters: 100 W radio frequency power, 50 sccm Ar flow, 5.4×10^{-3} mbar processing pressure, 30 min sputtering time. The ITO sputtering target was purchased from Kurt J. Lesker Company (In_2O_3/SnO_2 90/10 wt %). Hierarchical ITO structures were produced on the Ti strip following a published procedure.[9] Amino-TEMPO was covalently attached to ITO as described in our previous work[10]. IO-mesoITO electrodes for IMVs were functionalised following the same procedure as for amino-TEMPO but replacing 3-Phosphonopropionic acid with 3-Aminopropylphosphonic acid (for a positively charged surface) or 3-Phosphonopropionic acid (for a negatively charged surface). All electrochemical measurements were carried out using a Biologic potentiostat (BioLogic, UK) with EC-Lab software. All experiments were performed in degassed 150 mM PBS, adjusted to pH 7.0 (unless specified otherwise) at room temperature (20-25 °C). Ag wires were calibrated vs Ag|AgCl (3 M KCl) electrode (DRIREF-2, World Precision Instruments) by measuring the reduction potential of amino-TEMPO with both electrodes in a standard electrochemical cell in PBS 150 mM, pH 7.0. A new piece of Ag wire was used for each EPR tube (each FE-EPR cell) and had a calibrated shift of 100 ± 4 mV vs the Ag|AgCl DRIREF-2 electrode. The potentials measured with Ag wires were adjusted for this shift and converted vs SHE by adding 205 mV. The standard electrochemistry cell was purchased from Scientific Glassblowing Service of University of Southampton (dimensions on ESI Figure 3b).

4 Surface Characterisations

Scanning electron microscopy (SEM) images were collected using a Zeiss LEO Gemini 1525 FEG-SEM (field-emission-gun scanning electron microscope) with an InLens detector, using an accelerating voltage of 5 kV, 30 µm standard aperture, and 6.4 mm working distance. The analysis of pore size distribution based on SEM images was conducted using the Fiji ImageJ software. A Zeiss LSM 800 confocal laser scanning microscope (LSM) with Zen Blue 2.6 software was used to characterise ITO films on the Ti strips. The confocal reflection LSM stacks were obtained using a 405 nm laser (3.5% power) with a 20×/NA 0.7 objective lens. The collected stacks were then processed using ConfoMap software to obtain the 3D view image and determine the film thickness of the electrodes. X-ray photoelectron spectroscopy (XPS) spectra were recorded using a Thermo Scientific K-alpha$^+$ XPS spectrometer with a monochromated micro-focused Al Kα X-ray source (hν = 1486.6 eV) and a flood gun under an operating pressure of 2×10^{-7} mbar. The X-ray gun power was set to 72 W (6 mA and

12 kV) with a 400 µm spot size. The survey spectra were obtained using 200 eV pass energy, 0.5 eV step size, 25 ms dwell time and 3 scan accumulations. Charge correction was performed referring to the adventitious C1s peak at a binding energy of 284.8 eV.

The surface area of the IO-mesoITO electrode ($\boldsymbol{S}_{\text{IO-meso}}$) was estimated to be ca. 43 times higher than that of the mesoITO electrode ($\boldsymbol{S}_{\text{meso}}$) based on the following assumptions and calculations (see also ESI Figure 1):

1. For both type of electrodes, the shape of the ITO structure on Ti strip was considered to be a cuboid (length $\boldsymbol{a}$ = 45 mm, width $\boldsymbol{b}$ = 1 mm, thicknesses $\boldsymbol{c}$ individually determined by confocal microscopy detailed below);
2. For the mesoITO electrode, the only mesoporous structure accessible was considered to be the outer surface of the ITO cuboid ($\boldsymbol{S}_{\text{meso}} = \boldsymbol{ab} + 2\boldsymbol{bc}_1 + 2\boldsymbol{ac}_1$, thickness $\boldsymbol{c}_1$ = 13.2 µm);
3. For the IO-mesoITO electrode, the accessible mesoporous structure was considered to extend fully into the ITO cuboid (increased thickness $\boldsymbol{c}_2$ = 17.1 µm) due to interconnected macropores (pore size distribution peaked at ~640 nm);
4. The SEM image (length $\boldsymbol{x}$ = 57 µm, width $\boldsymbol{y}$ = 37 µm) was considered to be a 2D representation of the macropores distributed in a 3D 'SEM brick', with a thickness $\boldsymbol{z}$ estimated from the dominant macropore size distribution ($\boldsymbol{z}$ = 640 nm);
5. All the macropores in the 'SEM brick' were considered to be spherical and interconnected with each other, constituting a total surface area of 3300 µm^2 per SEM brick;
6. The size distribution of the macropores shown in the SEM brick represents the macropore distribution in the entirety of the IO-mesoITO cuboid;
7. The entirety of the IO-mesoITO cuboid is considered a stack of SEM bricks, with the quantity $\boldsymbol{n}$ calculated by dividing the volume of IO-mesoITO cuboid with the volume of one SEM brick ($\boldsymbol{n} = \boldsymbol{abc} / \boldsymbol{xyz}$);
8. The total surface area of the IO-mesoITO cuboid was estimated to be the quantity of SEM bricks $\boldsymbol{n}$ times the value of 3300 µm^2 per SEM brick plus the outer surface of the IO-mesoITO cuboid ($\boldsymbol{S}_{\text{IO-meso}} = \boldsymbol{n} \times 3300\ \mu m^2 + \boldsymbol{ab} + 2\boldsymbol{bc}_2 + 2\boldsymbol{ac}_2$).

5 EPR spectroscopic measurements and analysis

EPR measurements were performed in the Centre for Pulse Electron Paramagnetic Resonance spectroscopy (PEPR) located in the Department of Chemistry of Imperial College London. CW EPR spectra were recorded on a EMX spectrometer (Bruker) equipped with an ER 4122SHQE resonator and either a nitrogen variable temperature control unit (VTU) (for measurements with TEMPO) or a closed-circuit cryostat (Cryogenic Ltd.) controlled with a Lakeshore 350 temperature controller (for measurements with IMVs). The magnetic field was calibrated with DPPH as a standard (g = 2.0036)[11]. Microwave power, modulation amplitude and temperature are reported in the main text. All spectra were acquired under non-saturating conditions. All samples were prepared in Wilmad® quartz (CFQ) EPR tubes (Outer Diameter = 4 mm, length 10 mm)

6 Supplementary Table and Figures

ESI Table 1. Determination of the optimal position of the reference electrode in the FE-EPR cell. Uncompensated resistance (R_u) measured with impendence spectroscopy (ZIR) at open circuit potential on different sizes of electrodes and positions of reference electrode. The size and positioning of the reference electrode did not influence the measurements in the standard electrochemical cell. All measurements were performed in 150 mM PBS at pH 7.0. 'TOP', 'MID' and 'BOTTOM' refer to the positions as illustrated in ESI Fig. 3a.

RE position	Average R_u (Ω)
Working electrode with a width of 2 mm in EPR tube	
TOP	78.21
MID	35.88
BOTTOM	59.16
Working electrode with a width of 1 mm in EPR tube	
TOP	10.47
MID	4.47
Working electrodes with a width of 1 and 2 mm in standard cell	
Not significant	8.32

ESI Table 2. List of the principal parameters influencing the sensitivity and electrochemical properties of the PFE-EPR method.

Parameter	Effect	Solution	Reference
Resistance in the PFE-EPR cell	Increased uncompensated or solution resistance (total cell resistance); visible through large unexpected peak separation in cyclic voltammetry and/or sloping baseline in CVs	Reduce the dimensions of the working electrode, increase the concentration of electrolytes, reduce the distance between working and reference electrode	This study, 12, 13
Different particle sizes; different pore sizes; electrode surface characteristics	Problems with incorporation of the redox system, e.g. no redox peaks or EPR signals visible; maybe caused by insufficient or inhomogeneous absorption through multilayer formation hindering electron transfer	Size standardisation of the vesicles if the particles have a large size distribution; change the size of the pores in the ITO structure; change the surface charge of the ITO	14–17
Electron-transfer distance between site of interest and electrode surface Cofactor location in the membrane/ protein and orientation of the electrochemically active species	No or broad CV peaks; no EPR signals; apparent electron transfer constant derived from Nernst fittings n<<1	Attempt different immobilisation techniques to reduce electron-transfer distance; Quantify non electroactive species to 'rectify' Nernst plots; Consider electrochemical simulations to take into account different kinetics as a results of heterogenous immobilisation	This study, 18–22

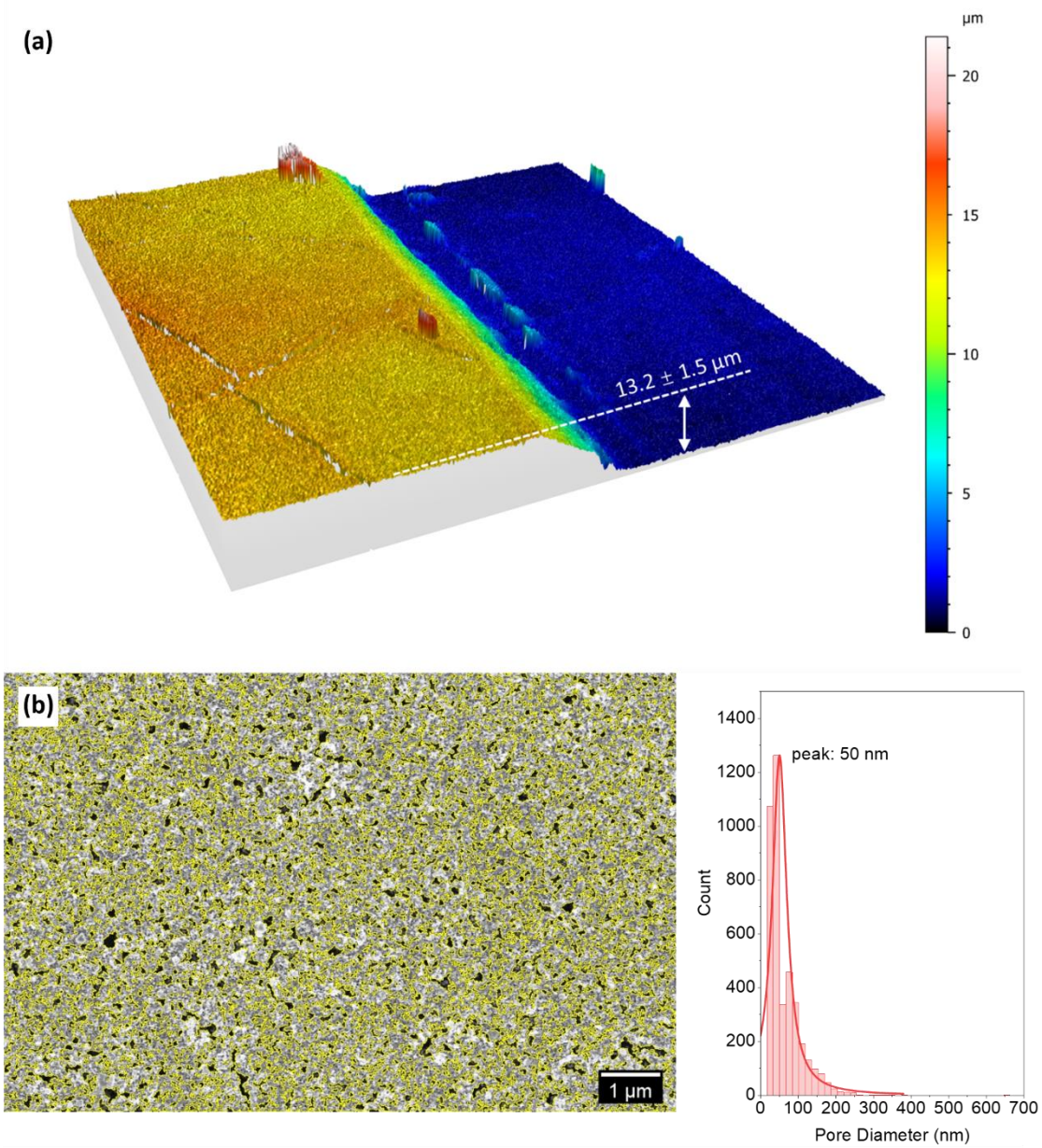

ESI Figure 1. Confocal surface 3D view, SEM images and pore size analysis for mesoITO working electrode surfaces. (a) Confocal 3D view, (b) SEM image at 2000 magnification with pore boundaries highlighted in yellow and (c) pore size distribution.

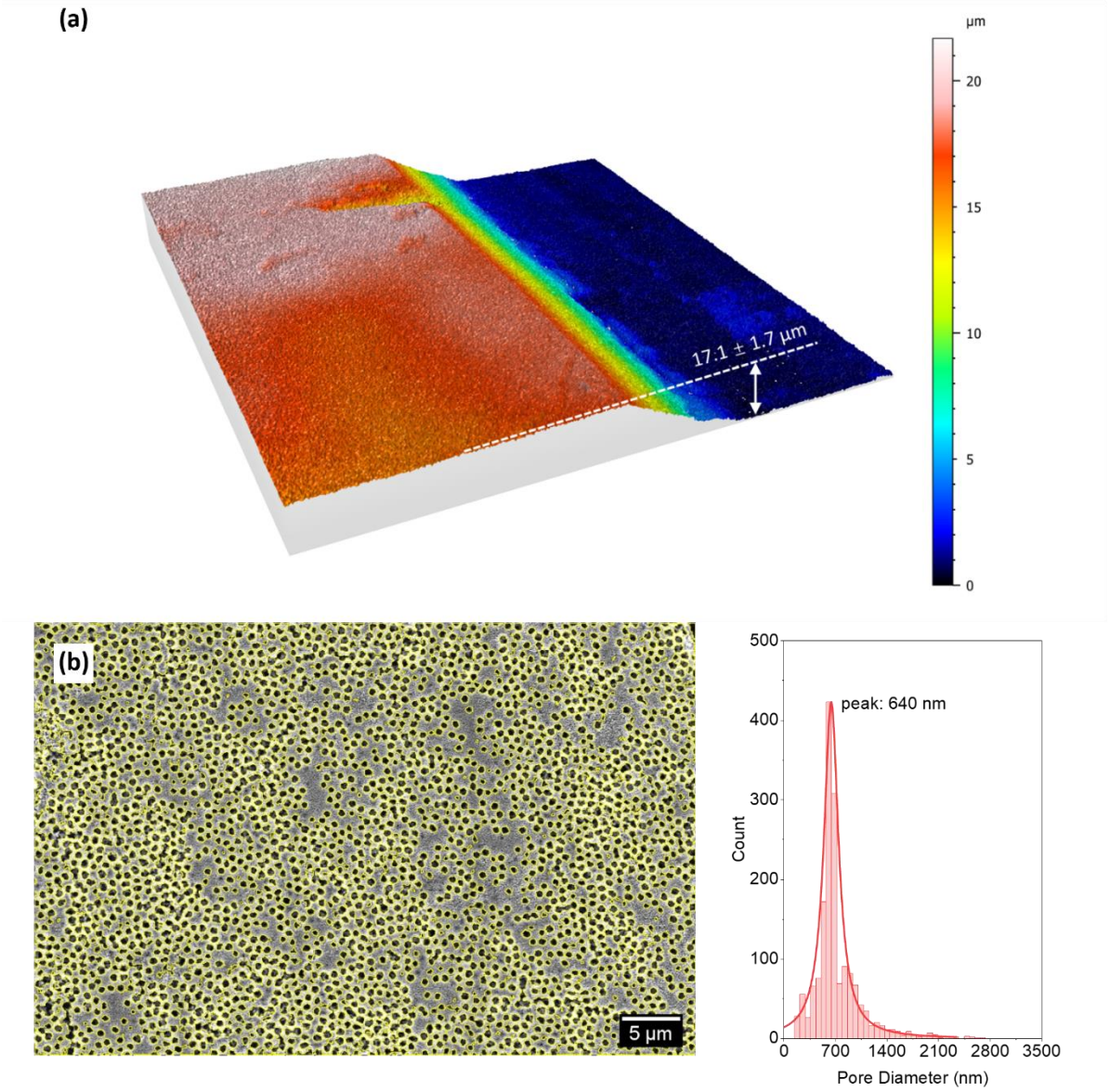

ESI Figure 2. Confocal surface 3D view, SEM images and pore size analysis for IO-mesoITO working electrode surfaces. (a) Confocal 3D view, (b) SEM image at 10000 magnification with pore boundaries highlighted in yellow and (c) pore size distribution. The magnification was selected to ensure that a statistically meaningful number of pores were included in the analysis to estimate the accessible surface area.

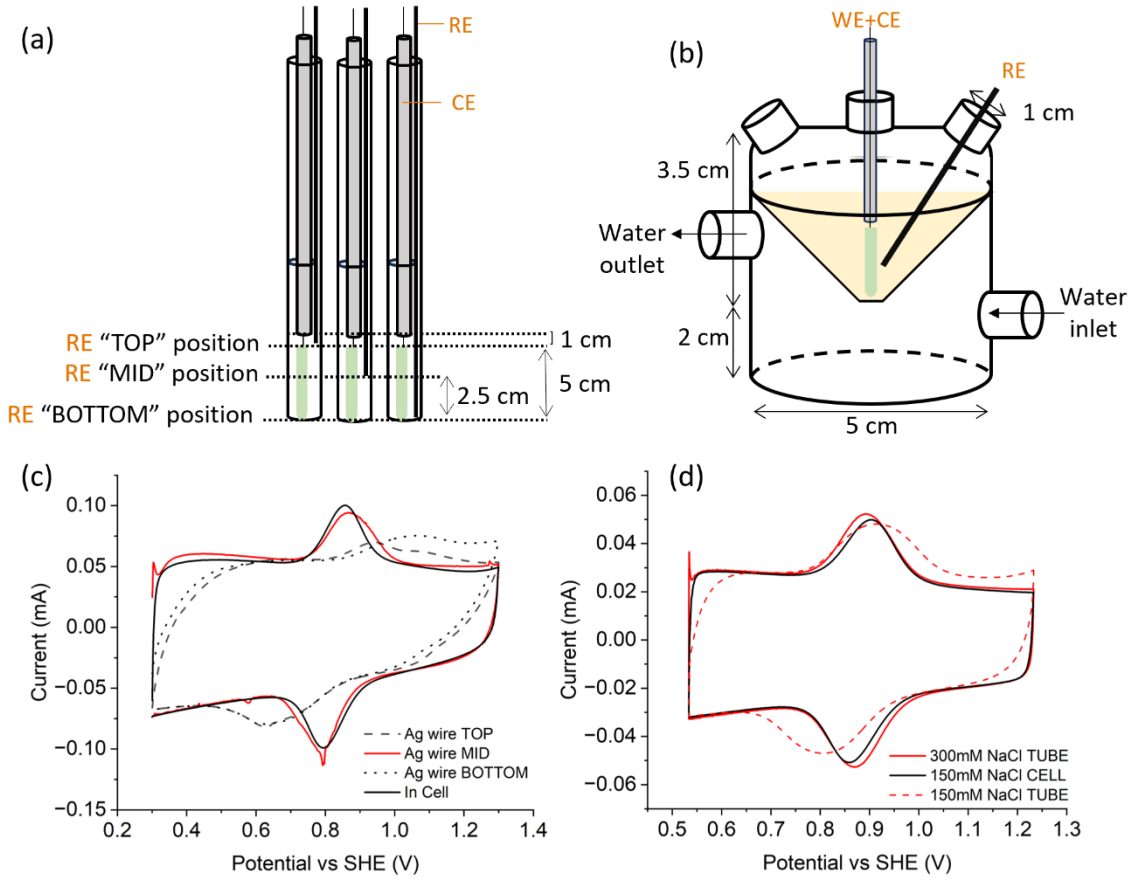

ESI Figure 3. Optimisation of the reference electrode (RE) position in the FE-EPR cell and effect of the ionic strength. Positioning of electrodes in (a) the EPR tube (b) and electrochemical cell (CE = counter electrode). (c) Cyclic voltammograms of amino-TEMPO functionalised mesoporous electrodes (2 mm width) with different positions of the reference electrode in the EPR tube compared to standard cell. (d) Cyclic voltammograms of electrodes (1 mm width) at different ionic strengths, all with the RE position as 'MID'. All CV scans were measured at 10 mVs^{-1} in 150 mM PBS buffer at pH 7.0.

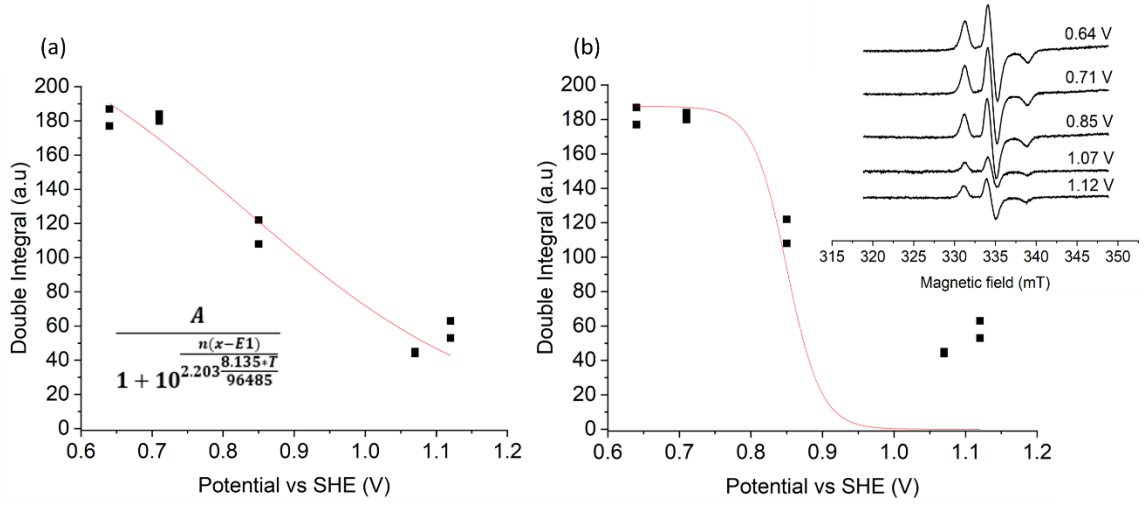

ESI Figure 4. Nernst curves of amino-TEMPO functionalised electrodes (1 mm width). (a) Converged fit with T = 298K, $E1$ = 0.85 V and n = 0.13. (b) Fit forced to n = 1. The Nernst equation is shown as an inset in (a). The inset in (b) shows the averaged EPR spectra recorded at 100 K.

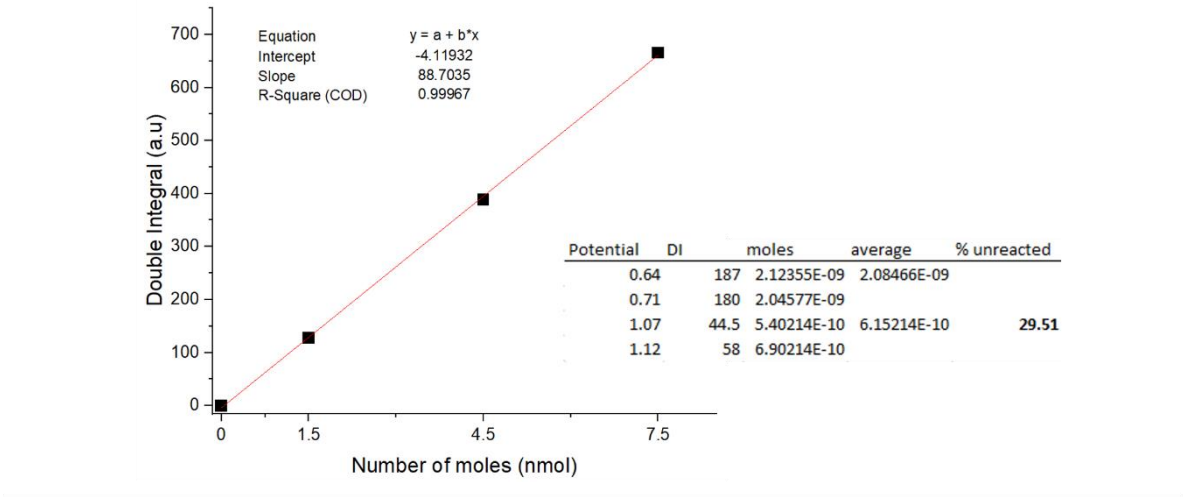

Potential	DI	moles	average	% unreacted
0.64	187	2.12355E-09	2.08466E-09	
0.71	180	2.04577E-09		
1.07	44.5	5.40214E-10	6.15214E-10	**29.51**
1.12	58	6.90214E-10		

ESI Figure 5. Calibration curve of amino-TEMPO in PBS 150 mM, pH 7.0 from 0 to 50 µM. Double integrals plotted versus nanomoles obtained by multiplying the molarity of the sample by the volume of solution in the tube (150 µL). The table shows the calculations for the estimation of unreacted TEMPO. Number of moles was calculated with the fitted equation using the double integral as "y". The percentage was calculated considering that the more reduced potentials have the maximum amount of TEMPO (which is not influenced by the potential applied) while the signal on the oxidised samples is only due to unreacted molecules.

SER^{210}– CYS^{14} distance = 52.01 Å (5.201 nm)

LYS^{203} – ALA^{37} distance = 53.93 Å (5.393 nm)

ILE^{171}– ARG^{2} distance = 46.02 Å (4.602 nm)

ESI Figure 6. Thickness of MsrQ estimated by distance measurements on the AlphaFold predicted tertiary structure (https://alphafold.com/entry/P76343). We have oriented the protein in different planes to show that its thickness is always higher than the inner membrane of *E.coli* (4 mm)[23] regardless of the orientation of MsrQ in the membrane. Green residues on the protein are the amino acids selected to measure the distance.

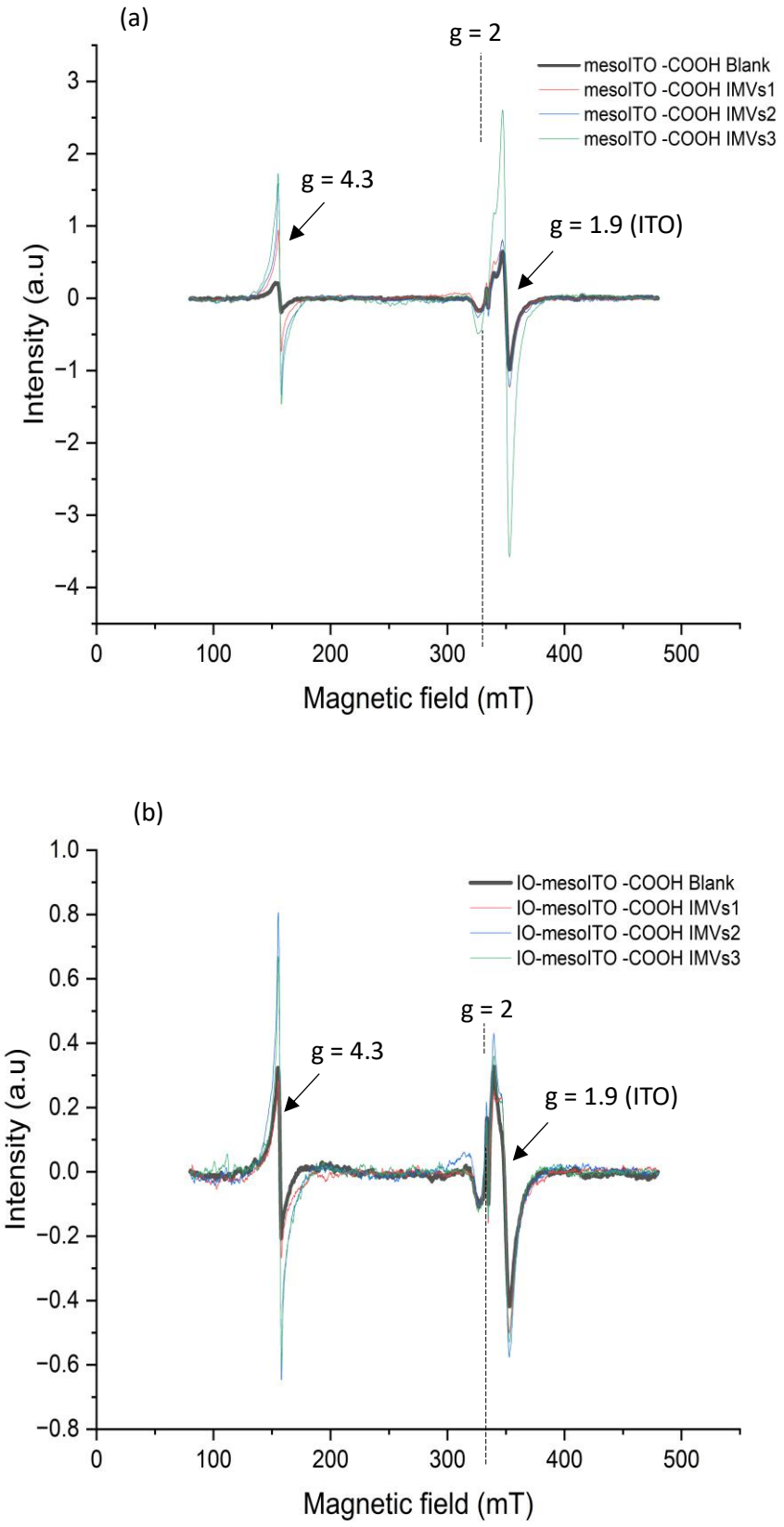

ESI Figure 7. CW EPR spectra of IMVs on (a) mesoITO and (b) IO-mesoITO working electrodes functionalised with 3-Phosphonopropionic acid. 10µL of the dispersion of IMVs (three repeats) at 30 mg/mL in MOPS 100 mM + EDTA 5 mM, pH 7.0 were drop-casted onto the working electrode. EPR spectra were recorded at 12 K, 1.8 mT modulation amplitude and 2 mW microwave power. The larger amount of free iron present in the IMV-treated samples originates from a contaminant in the buffer.

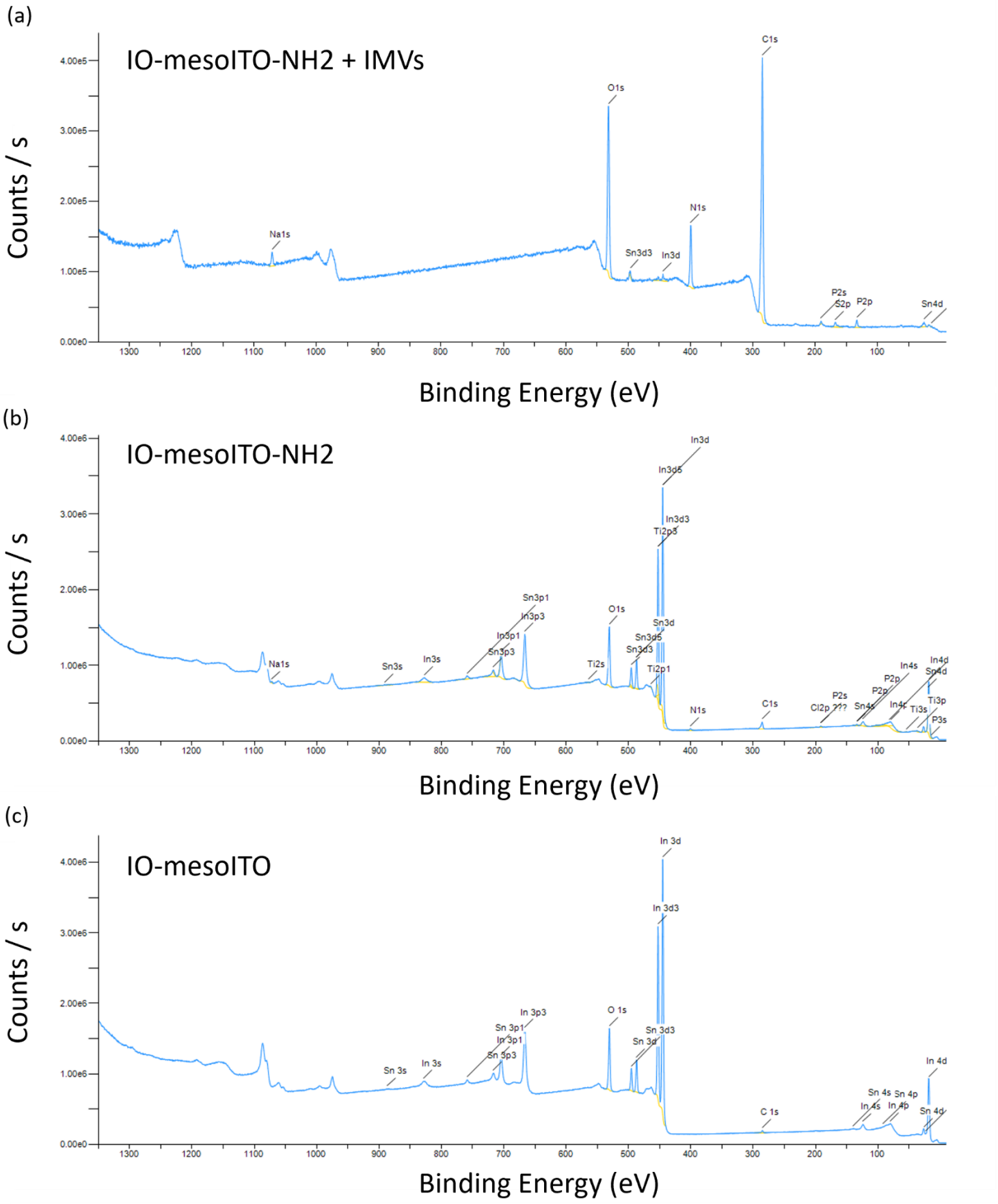

ESI Figure 7. XPS survey spectra. (a) IO-mesoITO functionalised with 3-Aminopropylphosphonic acid and with 10 µL of a 30 mg/mL dispersion of IMVs in PBS buffer pH 7.0 (150 mM); (b) IO-mesoITO functionalised with 3-Aminopropylphosphonic; (c) bare IO-mesoITO.

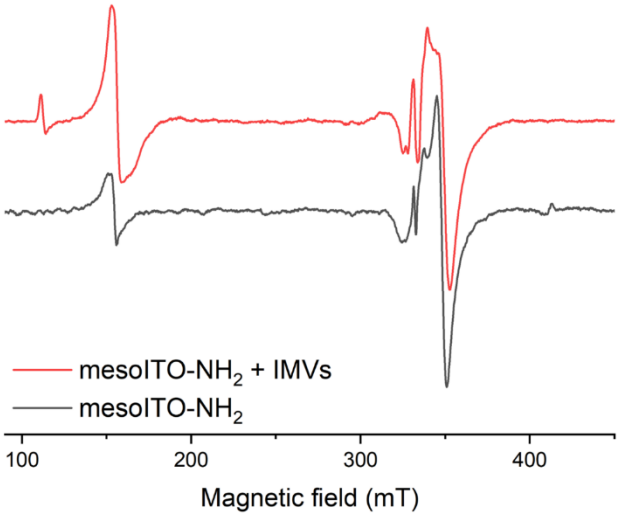

ESI Figure 8. CW EPR spectra of IMVs on mesoITO working electrodes. 10µL of the dispersion of IMVs at 30 mg/mL in MOPS 100 mM + EDTA 5 mM, pH 7.0 were drop-casted onto the working electrode. EPR spectra were recorded at 12 K. 1.8 mT modulation amplitude and 2 mW microwave power.

7 References

1 M. Kitagawa, T. Ara, M. Arifuzzaman, T. Ioka-Nakamichi, E. Inamoto, H. Toyonaga and H. Mori, Complete set of ORF clones of Escherichia coli ASKA library (A complete set of E. coli K-12 ORF archive): unique resources for biological research, *DNA Research*, 2005, **12**, 291–299.

2 M. Kitagawa, T. Ara, M. Arifuzzaman, T. Ioka-Nakamichi, E. Inamoto, H. Toyonaga and H. Mori, Complete set of ORF clones of Escherichia coli ASKA library (A complete set of E. coli K-12 ORF archive): unique resources for biological research, *DNA Research*, 2005, **12**, 291–299.

3 B. P. Rosen and T. Tsuchiya, Preparation of Everted Membrane Vesicles from Escherichia Coli for the Measurement of Calcium Transport, *Methods Enzymol*, 1979, **56**, 233–241.

4 S. Nir, J. Bentz, J. Wilschut and N. Duzgunes, Aggregation and fusion of phospholipid vesicles, *Prog Surf Sci*, 1983, **13**, 1–124.

5 W. Patrick, K. Shidong and J. Editors, *Extracellular Vesicles Methods and Protocols Methods in Molecular Biology 1660*, .

6 I. Yamato, Y. Anraku and K. Hirosawa, *Cytoplasmic Membrane Vesicles of Escherichia coli I. A Simple Method for Preparing the Cytoplasmic and Outer Membranes'*, 1975, vol. 77.

7 V. Prachayasittikul, C. Isarankura-Na-Ayudhya, T. Tantimongcolwat, C. Nantasenamat and H. J. Galla, EDTA-induced membrane fluidization and destabilization: Biophysical studies on artificial lipid membranes, *Acta Biochim Biophys Sin (Shanghai)*, 2007, **39**, 901–913.

8 C. R. Harrington, Lowry protein assay containing sodium dodecyl sulfate in microtiter plates for protein determinations on fractions from brain tissue, *Anal Biochem*, 1990, **186**, 285–287.

9 M. Kato, T. Cardona, A. W. Rutherford and E. Reisner, Photoelectrochemical water oxidation with photosystem II integrated in a mesoporous indium-tin oxide electrode, *J Am Chem Soc*, 2012, **134**, 8332–8335.

10 K. Abdiaziz, E. Salvadori, K. P. Sokol, E. Reisner and M. M. Roessler, Protein film electrochemical EPR spectroscopy as a technique to investigate redox reactions in biomolecules, *Chemical Communications*, 2019, **55**, 8840–8843.

11 J. Krzystek, A. Sienkiewicz, L. Pardi and L. C. Brunel, *DPPH as a Standard for High-Field EPR*, 1997, vol. 125.

12 Y. Zhang, B. Zhang and H. S. White, Electrochemistry of nanopore electrodes in low ionic strength solutions, *Journal of Physical Chemistry B*, 2006, **110**, 1768–1774.

13 G. M. Tom, A. T. Hubbard, J. Electroanal Chem, F. C. Anson, R. A. Osteryoung, D. M. Oglesby, J. D. Johnson, C. N. Reilley and E. Schmidt, *Thin Layer Electrochemistry Minimization of Uncompensated Resistance*, UTC, 1969, vol. 22.

14 L. J. C. Jeuken, S. D. Connell, M. Nurnabi, J. O'Reilly, P. J. F. Henderson, S. D. Evans and R. J. Bushby, Direct electrochemical interaction between a modified gold electrode and a bacterial membrane extract, *Langmuir*, 2005, **21**, 1481–1488.

15 V. A. Hernández and F. Scholz, The Electrochemistry of Liposomes, *Isr J Chem*, 2008, **48**, 169–184.

16 K. P. Sokol, D. Mersch, V. Hartmann, J. Z. Zhang, M. M. Nowaczyk, M. Rögner, A. Ruff, W. Schuhmann, N. Plumeré and E. Reisner, Rational wiring of photosystem II to hierarchical indium tin oxide electrodes using redox polymers, *Energy Environ Sci*, 2016, **9**, 3698–3709.

17 X. Fang, K. P. Sokol, N. Heidary, T. A. Kandiel, J. Z. Zhang and E. Reisner, Structure-Activity Relationships of Hierarchical Three-Dimensional Electrodes with Photosystem II for Semiartificial Photosynthesis, *Nano Lett*, 2019, **19**, 1844–1850.

18 J. N. Butt, L. J. C. Jeuken, H. Zhang, J. A. J. Burton and A. L. Sutton-Cook, Protein film electrochemistry, *Nature Reviews Methods Primers*, , DOI:10.1038/s43586-023-00262-7.

19 M. Jaugstetter, N. Blanc, M. Kratz and K. Tschulik, *Chem Soc Rev*, 2022, 51, 2491–2543.

20 M. J. Eddowes and H. O. Allen Hill, *Eddowes, Hill / Electrochemistry of Horse Heart Cytochrome c Electrochemistry of Horse Heart Cytochrome c*, UTC, 2024, vol. 16.

21 J. Vacek, M. Zatloukalova and D. Novak, *Curr Opin Electrochem*, 2018, 12, 73–80.

22 F. A. Armstrong, R. M. Evans, S. V. Hexter, B. J. Murphy, M. M. Roessler and P. Wulff, Guiding Principles of Hydrogenase Catalysis Instigated and Clarified by Protein Film Electrochemistry, *Acc Chem Res*, 2016, **49**, 884–892.

23 A. Briegel, D. R. Ortega, E. I. Tocheva, K. Wuichet, Z. Li, S. Chen, A. Mü Ller E, C. V Iancu, G. E. Murphy, M. J. Dobro, I. B. Zhulin and G. J. Jensen, *Universal architecture of bacterial chemoreceptor arrays*, 2009.